WESTERN REGION TECHNICAL ATTACHMENT
NO. 98-15
APRIL 14, 1998

THE OBSERVATION OF A SUPERCELL THUNDERSTORM OVER HIGH TERRAIN IN NORTHERN ARIZONA

Tony Perez - NWSO Flagstaff

Abstract

Radar data collected on 2 September 1996 documented the occurrence of a possible supercell thunderstorm over the high terrain of northern Arizona. The environmental conditions shown by the modified sounding, 35 km from the thunderstorm location, revealed a CAPE of 1386 J kg^{-1}. The observed storm motion to the *west* at 20 m s^{-1} resulted in a storm-relative helicity in the 0-3 km layer of 344 m^2 s^{-2}. Several reflectivity and velocity signatures typically associated with supercells were observed in this storm. Doppler storm-relative velocity data showed a deep mesocyclone lasting for over 90 minutes. Reflectivity data showed a low-level hook echo, updraft overhang and a mid-level "v-notch" located downstream from the updraft. The storm's orientation and movement differed significantly from typical supercell thunderstorms observed across the Great Plains, however, the storm motion was found to be to the right of the mean wind shear vector. Due to the complex terrain and the distance of the radar to the thunderstorm, however, it is not conclusive whether the internal storm dynamics or external influences contributed to the rightward propagation of this storm. This Technical Attachment (TA) describes one of the first supercell thunderstorms documented in the complex high terrain of Arizona.

Introduction

Few supercell thunderstorms are documented west of the Rocky Mountains (see Moller et al. 1994; Monteverdi and Johnson 1996; Graham and Staudenmaier 1997). Although climatological conditions in this part of the country support a lower supercell frequency, a mature supercell occurring in the proper environment in the complex terrain of the West can be as destructive as a "Plains" type supercell. Until the deployment of the National Weather Service (NWS) radar and satellite observing networks, supercell storms in the sparsely populated and mountainous terrain west of the Rocky Mountains went largely unnoticed. Due in part to their rarity, supercells continue to be a forecasting challenge in this region of the United States. In a select list of 40 notable supercell events, Moller et al.,

(1994) identified two events that occurred along the Front Range or west of the Rocky Mountains. Monteverdi and Johnson (1996) observed a supercell thunderstorm in California's San Joaquin Valley. This storm produced hail as large as 2.9 cm (11/8 in.) and unconfirmed reports indicated larger hailstones. Graham and Staudenmaier (1997) documented a case of a splitting supercell in southeast Idaho and stressed the importance of hodograph structure for anticipating convection. These reports recognize the difficulties associated with identifying severe thunderstorms due to the different environmental conditions supporting these storms coupled with the observing limitations introduced by the mountainous terrain. This TA will document an additional high elevation supercell case, first investigated by Keighton and Passetti (1998) which occurred over the complex terrain of northern Arizona's Mogollon Rim. The elevation of the terrain in this region is approximately 2330 m (7000 ft) MSL.

This thunderstorm occurred on 2 September 1996 approximately 16 km southeast of Flagstaff and 80 km from the KFSX WSR-88D in southern Coconino County. Observations of funnel clouds, heavy rainfall, and 2.5 cm hail were reported near this thunderstorm. The elevation of the heavily wooded terrain over which the thunderstorm developed was around 2330 m (7000 ft). As the storm traveled westward over several canyons and other regions of complex terrain, the mean elevation sloped downward to reach 2160 m (6500 ft). Figure 1 shows the storm path, the location of the KFSX radar, the radiosonde launch site at the NWS field office (NWSO FGZ), and general surface terrain. Since this thunderstorm traveled over largely unpopulated and rugged terrain, it was difficult to estimate how, if at all, the complexities in the terrain contributed to turning this storm to the right of the mean wind shear vector. Data collected for this event suggested that clockwise curvature in the lowest few kilometers of the hodograph may have influenced this movement to the right of the mean wind shear vector as in the case modeled by Klemp and Wilhelmsen (1978). The instability revealed by the morning sounding and wind profile of the corresponding hodograph suggested organized convection was likely to occur later in the day. A deep and persistent mesocyclone and several reflectivity signatures often attributed to supercells were identifiable in the storm relative velocity and base reflectivity data from the KFSX radar. The available data suggested that the observed thunderstorm may be the first documented supercell storm to occur in the high terrain of northern Arizona.

General Supercell Characteristics

Supercell thunderstorms are generally associated with winds which not only increase with height but also veer strongly with height (Browning, 1964). The classic Plains supercell is often depicted with a clockwise curving hodograph and a storm movement from the west-southwest. Klemp and Wilhelmsen (1978) and Weisman and Klemp (1984) demonstrated the important influence of directional shear on modeled supercell storms. In particular, clockwise curvature in the low levels of a hodograph favored the rightward movement of a modeled split supercell pair. Similarly, counterclockwise curvature sustained the leftward moving cell. Brown (1990) depicts a composite hodograph, shown in Fig. 2a, derived from 28 Great Plains supercell thunderstorms displaying a rightward moving tendency. In this composite hodograph, the mean wind shear vector for 0-6 km AGL points from the west

to east and the anticipated storm motion would be to the right of this vector, or from the southwest. The near-surface storm features associated with such a hodograph are described in Lemon and Doswell (1979) and the familiar plan view schematic diagram is shown in Fig. 2b. With such an orientation and direction of movement, the hook echo, mesocyclone and updraft are located along the "rear" flank of the storm. Different hodograph positions, however, have interesting implications for the corresponding storm orientation and direction of movement. Figure 3 shows three possible clockwise-curving hodograph positions and resulting storm motions for right-moving supercells. The thin arrows in this figure represent the estimated mean wind shear vector. The circles positioned on this vector are estimates of the mean wind speed. The resulting storm motion can be estimated by moving to the right of this circle, representing the mean wind speed, orthogonal to the mean wind shear vector. The heavy arrow in each example represents the approximate storm motion. On the right side, Fig. 3 shows the low-level reflectivity orientation and storm motion based on the storm-relative flow for each example. The resulting storm motion depends on the position of the hodograph relative to the origin, which also defines the forward flank of the storm.

Supercell thunderstorms are often associated with multiple reflectivity signatures. These include, but are not limited to, an overhanging mid-level echo, an updraft "vault" and a hook echo at low levels. Weisman and Klemp (1986) describe the evolution of a typical supercell in three phases. The first phase of supercell development is similar to single cell growth in which the radar reflectivity pattern is vertically aligned and the storm motion is generally in the direction of the mean wind. The next stage of development, tens of minutes later, is associated with an elongation of the mid-level reflectivity pattern in the direction of the mean wind shear vector and by a strong reflectivity gradient on the southwest flank. Additionally, the mid-level reflectivity field overhangs the low-level reflectivity field on the southwest flank, indicating the presence of a strong updraft. During this phase, the storm moves to the right of the mean wind. During the supercell's mature stage, a hook-like appendage appears on the southwest flank of the storm and the mid-level echo overhang is still present.

These features were identifiable in the northern Arizona thunderstorm observed and recorded by the KFSX radar. The orientation of these features were different, however, relative to the westward storm motion, and were contrary to what is expected from the more commonly observed and documented Plains supercells. Analysis of the environmental winds helped to explain the relative positions of these features. The bottom component of Fig. 3 indicates that the hook echo, mesocyclone, and updraft would be located on the forward flank of the storm. This example most resembles the supercell storm discussed in this paper. Consequently, the hook echo, main updraft, and mesocyclone were located on the *forward* flank as this storm moved to the west. With a firm conceptual understanding of supercell environments and internal storm circulation, forecasters can anticipate the behavior of these thunderstorms given a reasonably representative hodograph.

Pre-storm Environment

The synoptic weather pattern associated with this Arizona thunderstorm was typical for the time of year. Subtle features leading up to this event included a shortwave trough, embedded within a flat ridge over the Southwest, and a moist southerly surface flow. The shortwave moved to the east, maintaining a dry northwesterly flow at 500 hPa through the afternoon. Although the lower atmosphere was relatively dry, the southerly surface winds helped to maintain a dew-point temperature in Flagstaff around 8°C (47°F) at 1900 UTC. A shallow layer of moist air near the surface, combined with strong instability and a favorable hodograph shape helped to support organized convection.

a. FGZ Sounding and hodograph

Observations from the 1200 UTC FGZ sounding and hodograph indicated a high potential for afternoon thunderstorms. The observed and modified FGZ soundings are shown in Fig. 4. The value of CAPE associated with the observed sounding was approximately 1500 J kg^{-1} and the modified sounding resulted in a CAPE value of almost 1400 J kg^{-1} for parcels lifted from the surface. Above 500 hPa, a capping inversion was strong enough only to delay convection until the early afternoon. The inversion around 700 hPa shown in Fig. 4a eroded by the late morning as surface heating mixed the boundary layer air.

Clues for this behavior were evident in the observed and modified FGZ hodographs, shown in Fig. 5, which showed strong directional shear. The 0-6 km winds curved clockwise with height. At 1900 UTC, surface winds were observed from the west around 10 m s^{-1}. 600 hPa winds were from the northwest at 40 m s^{-1} and the 500 hPa winds were from the north-northeast at 36 m s^{-1}. Above this altitude, winds backed to the west with upper-level winds reaching almost 120 m s^{-1}. The observed storm motion was to the west at 20 m s^{-1}. Consequently, the storm-relative helicity in the 0-3 km layer was 344 m^2 s^{-2}. This value is over twice the minimum threshold for tornadoes of 150 m^2 s^{-2} suggested by Davies-Jones et al (1990). The strong directional shear of the clockwise curvature of the hodograph helped sustain long-lived convection for this thunderstorm. Since the hodograph was located approximately 35 km from the storm location and with the complexity of the surrounding terrain, it is uncertain whether or not the low-level hodograph structure is truly representative of the actual conditions near this storm. The observed behavior of the storm, however, seems to fit this hodograph structure.

b. Radar characteristics

Around 1900 UTC, the first cells appeared on KFSX radar approximately 80 km from the radar site, or approximately 16 km southeast of Flagstaff. For over one hour, these storms developed vertically with no apparent motion deviating from the mean wind. At 2036 UTC, the first signs of motion or development to the west were observed. Supercell characteristics associated with this cell were evident until approximately 2241 UTC. These characteristics included a hook echo, strong updraft overhang at mid levels, and a reflectivity v-notch at mid levels. The velocity imagery indicated the presence of a deep mesocyclone and a resulting storm motion to the right of the mean wind shear vector.

1) Reflectivity

Vertically aligned echoes were apparent on the KFSX WSR-88D at 1901 UTC. Reflectivity values associated with this cluster of storms reached 50 dBZ as the cells propagated slowly to the south. Over one hour later at 2023 UTC, elongation of the mid-level reflectivity field was apparent and were possibly associated with a maturing supercell (Weisman and Klemp, 1986). Figure 6 shows three consecutive volume scans for two different elevation angles sampling the storm at 2970 m (8900 ft) and 4000 m (12000 ft) AGL. The circle shown in the figures is only a fixed reference point for identifying storm features. This sequence of panels reveals the elongated reflectivity pattern as targets within the thunderstorm updraft were pushed windward in the direction of the mean wind shear vector. From volume scans 219 through 221, reflectivities greater than 50 dBZ are shown along a line to the southeast of the reference marker.

At 2141 UTC, additional reflectivity signatures attributed to supercells were identifiable. Figures 7a-b show evidence of a hook echo, the positions of the main downdraft regions, an updraft overhang and a reflectivity v-notch. The lowest elevation slice in Fig. 7a shows data at 970 m (2900 ft) AGL and the second panel, Fig. 7b, shows data around 6100 m. Fig. 7a reveals a hook echo to the northwest of the circle reference marker. Reflectivity values associated with this appendage were over 55 dBZ and surrounding the reference point, in the weak echo region (WER), reflectivity was approximately 20 dBZ. Fig. 7b shows strong reflectivity overhang associated with the updraft. Reflectivity values surrounding the reference marker, 5000 m higher, were approximately 55 dBZ. A reflectivity v-notch is also shown in Fig. 7b. The mean wind associated with this case was from the north-northwest and its interaction with the strong updraft resulted in this commonly observed "v" reflectivity pattern at mid levels. This pattern is shown just to the southeast of the reference marker.

Figure 7a also relates the unexpected nominal positions of the main downdraft regions. These regions of high reflectivity correspond to the positions of the front and rear flank downdrafts shown in Fig. 2b. To the northwest of the reference marker, a region of high reflectivity comprising the hook appendage was considered one of the main downdrafts. This downdraft region was located on the forward flank of the thunderstorm with respect to the storm motion. A broad area from the north-northeast to the southeast, on the rear flank of the storm, was considered the second downdraft region. Compared to the orientation of a Plains supercell, the front and rear flank of this storm were contrary to what is typically expected and references to the "front" and "rear" flank downdrafts may be misleading. Since this storm was moving to the west-northwest, the updraft, hook echo, and mesocyclone were along the front flank.

2) Velocity

Doppler velocity images from the KFSX radar showed a deep and persistent mesocyclone associated with this thunderstorm. The radar's mesocyclone detection algorithm identified

mesocyclonic circulation as early as 2046 UTC. Figure 8 shows the storm-relative velocity imagery valid at this time in which the low-level wind field showed cyclonic convergence. At upper levels, near 12330 m (34100 ft), the wind field at the storm top was divergent. This mesocyclonic circulation was also evident in cross sections of the storm-relative velocity field. This sequence of panels also shows how the updraft tilted to the southeast at higher elevations within the storm. The center of the mesocyclonic flow is farther to the southeast in each of the panels. Figure 9 shows the low-level convergence sustaining the updraft. In this figure, the radar is located 90 km to the right of the image. Near the top of the figure, strong divergence was shown near 12330 m AGL. During its mature stage, the mesocyclonic flow was more clearly visible. Figure 10a-d shows four panels of storm-relative velocity data valid at 2136 UTC. The yellow circle represents the radar-defined mesocyclone circulation. Panel 10a shows convergence at 970 m. Panel 10b shows cyclonic convergence at 3630 m. At 6200 m, panel 10c shows cyclonic rotation and the last panel, Fig. 10d, pure divergence was evident near the storm top at 10570 m. These patterns were visible for several volume scans and finally disappeared around 2216 UTC. The mesocyclone detection algorithm maintained a mesocyclone alert until 2207 UTC.

The close timing of the development of the mesocyclone circulation and the propagation of the storm to the west suggested that internal storm dynamics influenced the storm's turn to the right. There is evidence, however, of a gust front which spread south and west of the main storm at 2111 UTC. Although it is possible that the outflow boundary influenced the westward propagation of this storm, it is not conclusive. An outflow boundary reflectivity signature is not evident until approximately 30 minutes after the storm began moving to the right.

Conclusion

Radar data collected 2 September 1996 documented the occurrence of an apparent supercell thunderstorm over the rugged, high-elevation terrain of northern Arizona. The environmental conditions revealed by the morning sounding at FGZ, although 35 km from the thunderstorm location, indicated both strong instability and directional wind shear for that day. Several reflectivity and velocity signatures also supported this observation. Reflectivity data showed evidence of a low-level hook echo, updraft overhang, and mid-level v-notch downstream from the updraft. The storm relative velocity data showed a deep and persistent mesocyclone that lasted for over 90 minutes. Although the storm's orientation and movement differed from supercell thunderstorms observed across the Plains, careful hodograph analysis and interpretation offered the opportunity to anticipate this behavior. Due to the complex terrain and the distance of the thunderstorm to the radar, however, it is still not clear if the internal storm dynamics or external influences contributed to the rightward propagation of this storm.

References

Brown, R. A., 1990: Characteristics of supercell hodographs. *Preprints: 16th Conf. on Severe Local Storms,* Kananaskis, Alberta, Amer. Meteor. Soc., 30-33.

Browning, K. A., 1964: Airflow and precipitation trajectories within severe local storms which travel to the right of the mean winds. *J. Atmos. Sci.*, **21**, 634-639.

Davies-Jones, R., D. Burgess, and M. Foster, 1990: Test of helicity as a tornado forecast parameter. *Preprints: 16th Conf. on Severe Local Storms*, Kananaskis, Alberta, Amer. Meteor. Soc., 588-592.

Graham, R., and M. Staudenmaier, Jr., 1997: The severe weather event of 18 June 1997: an example of splitting supercells. NOAA Tech. Memo. NWS-WR 97-39.

Keighton, S. K. and V. Passetti, 1998: Anticipation and observation of a northern Arizona supercell over high terrain. *Preprints: 16th Conf. on Weather Analysis and Forecasting*, Phoenix, Arizona, Amer. Meteor. Soc., 124-126.

Klemp, J. B., and R. B. Wilhelmsen, 1978: The simulation of three-dimensional convective storm dynamics. *J. Atmos. Sci.*, **35**, 1070-1096.

Lemon, L. R. and C. A. Doswell III, 1979: Severe thunderstorm evolution and mesocyclone structure as related to tornadogenesis. *Mon. Wea. Rev.*, **107**, 1184-1197.

Moller, A. R., C. A. Doswell, M. P. Foster and G. R. Woodall, 1994: The operational recognition of supercell thunderstorm environments and storm structures. *Wea. Forecasting*, **9**, 327-347.

Monteverdi, J. P. and S. Johnson, 1996: A supercell thunderstorm with hook echo in the San Joaquin Valley, California. *Wea. Forecasting*, **11**, 246-261.

Weisman, M. L. and J. B. Klemp, 1984: The structure and classification of numerically simulated convective storms in directionally varying wind shears. *Mon. Wea. Rev.*, **112**, 2479-2498.

_____, 1986: Characteristics of isolated convective storms. *Mesoscale Meteorology and Forecasting*, P. S. Ray, Ed., Amer. Meteor. Soc., 331-358.

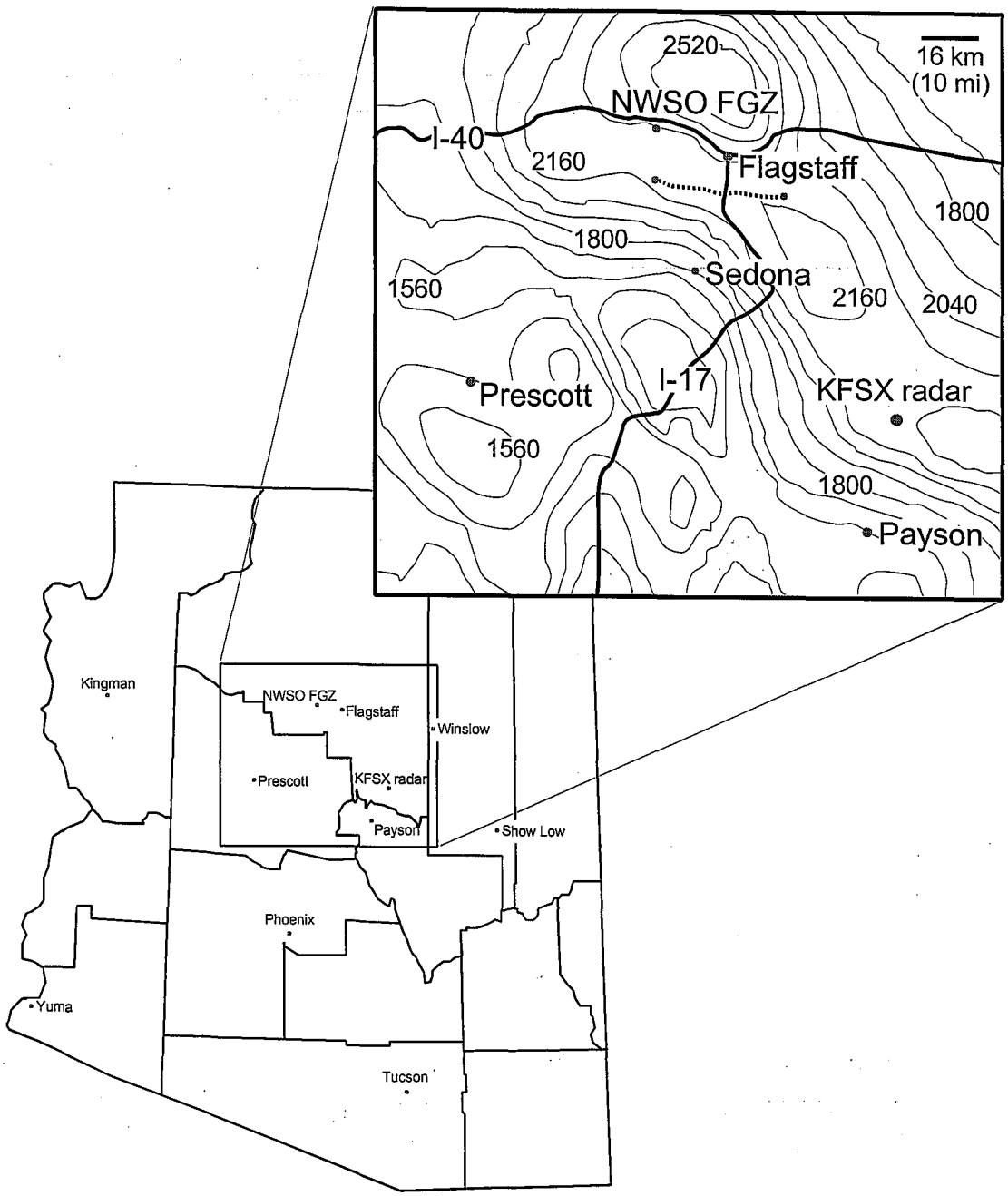

Fig. 1. Map of Arizona with selected counties outlined. Major cities and towns are identified. The inset shows terrain contours (thin lines) at 120 m intervals. Selected contours are labeled in meters. Heavy lines are interstate highways. The dotted line represents the supercell track.

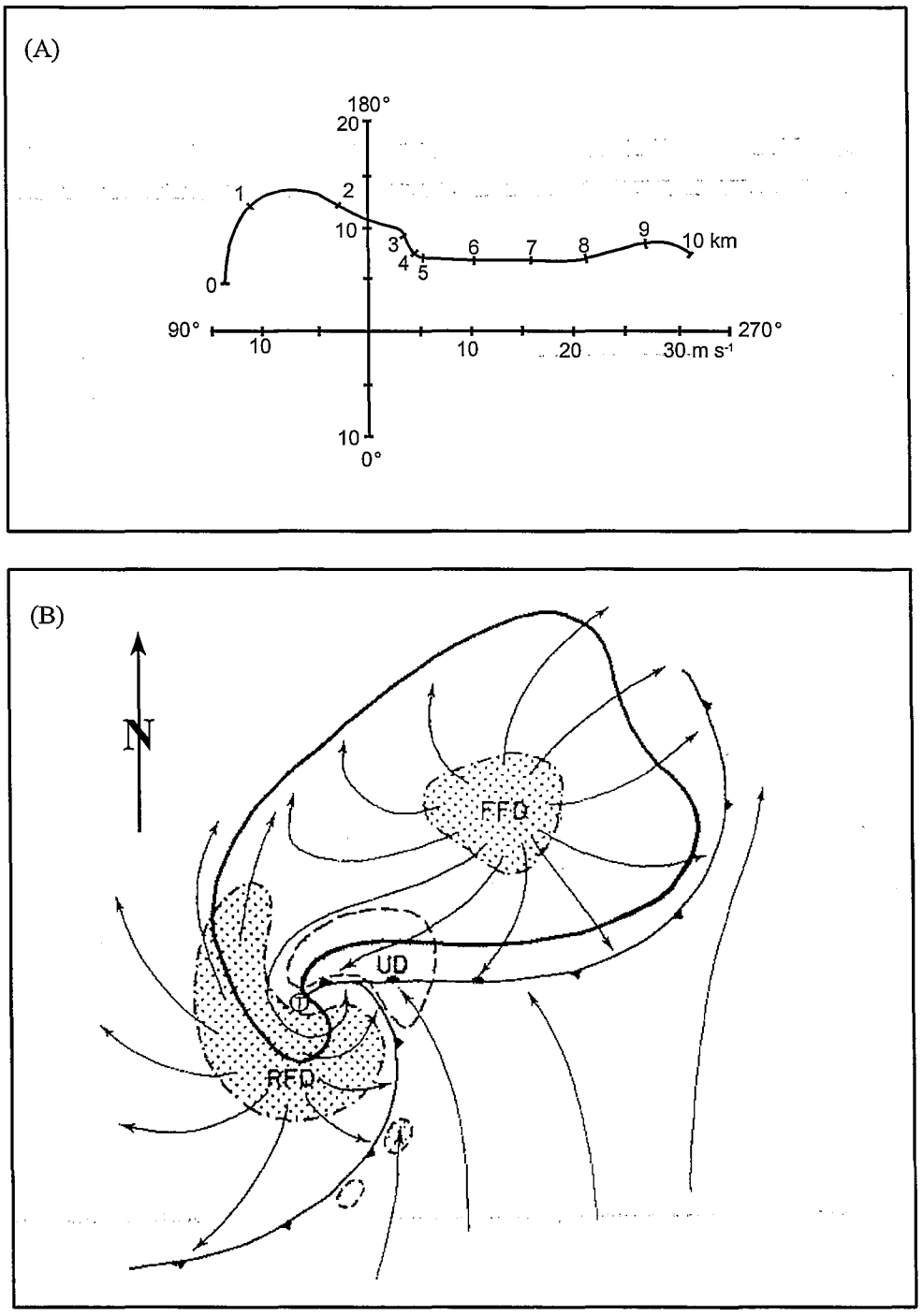

Fig. 2. (A) Composite storm-relative hodograph developed from 28 Great Plains supercells. Ticks along profile are labeled in km. Velocity scale in m s^{-1}. (From Brown, 1990). Part (B) shows a schematic plan view of a supercell at the surface. The thick line encompasses the radar echo. Dashed lines show the updraft position (labeled "UD"); the forward flank and rear flank downdrafts ("FFD" and "RFD", respectively) are lightly stipled; arrows are ground-relative streamlines. Storm motion is from the southwest. (From Lemon and Doswell, 1979).

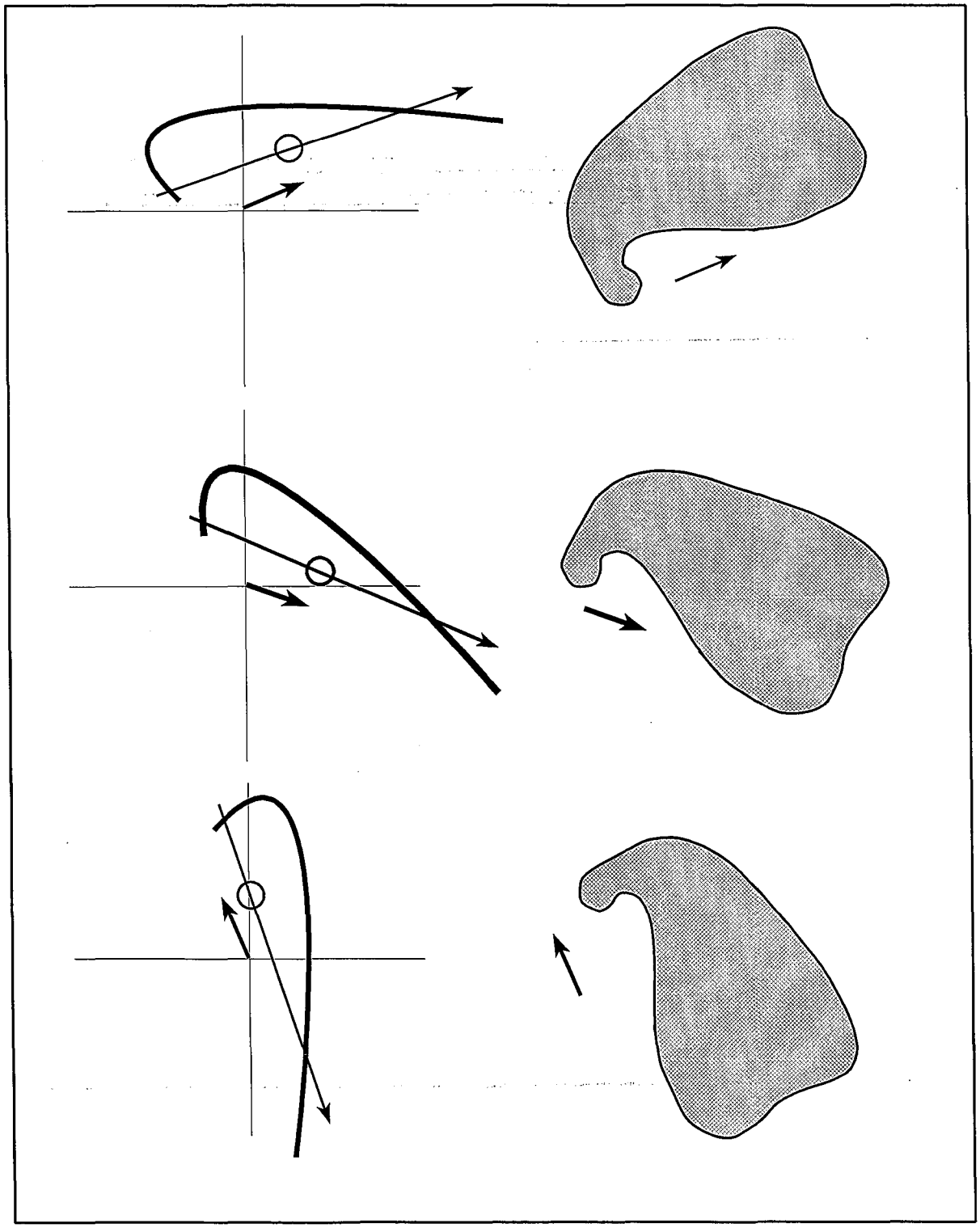

Fig. 3. Three different clockwise curving hodograph shapes and the resulting storm motions. The long, thin arrow on each hodograph represents the mean wind shear vector. The circle positioned along this vector represents the estimated mean wind speed. The heavy arrow extending from the origin indicates the computed mean storm motion. On the right side of the figure, the low-level reflectivity corresponding to the various hodograph shapes are shown. The heavy arrows are the same as the mean storm motions shown on each hodograph. (Adapted from Keighton and Passetti, 1998).

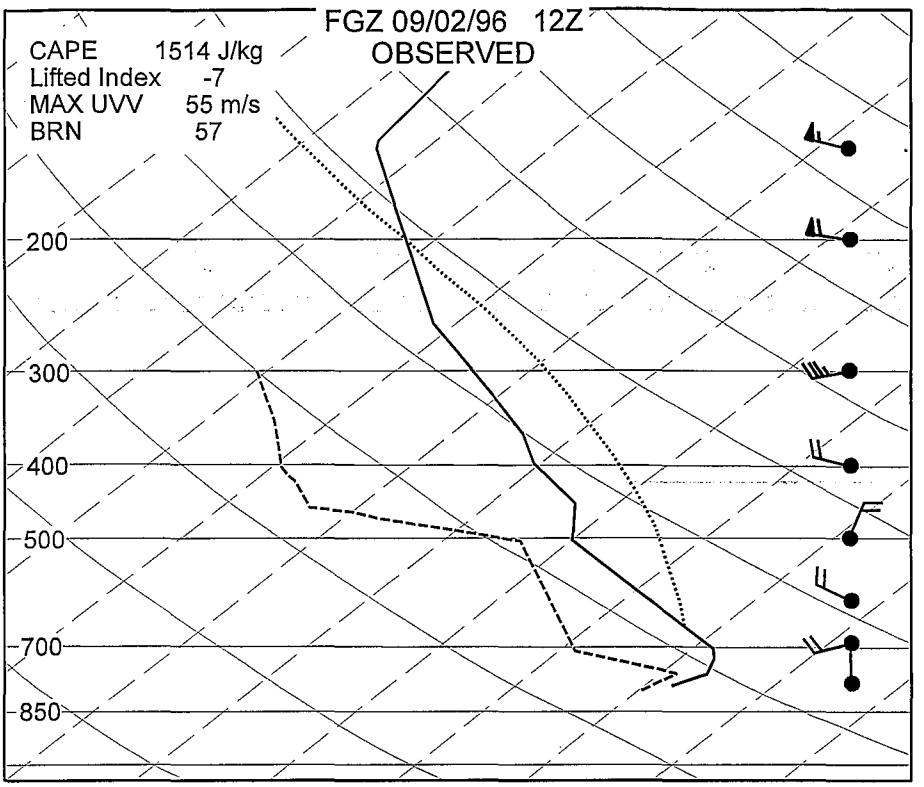

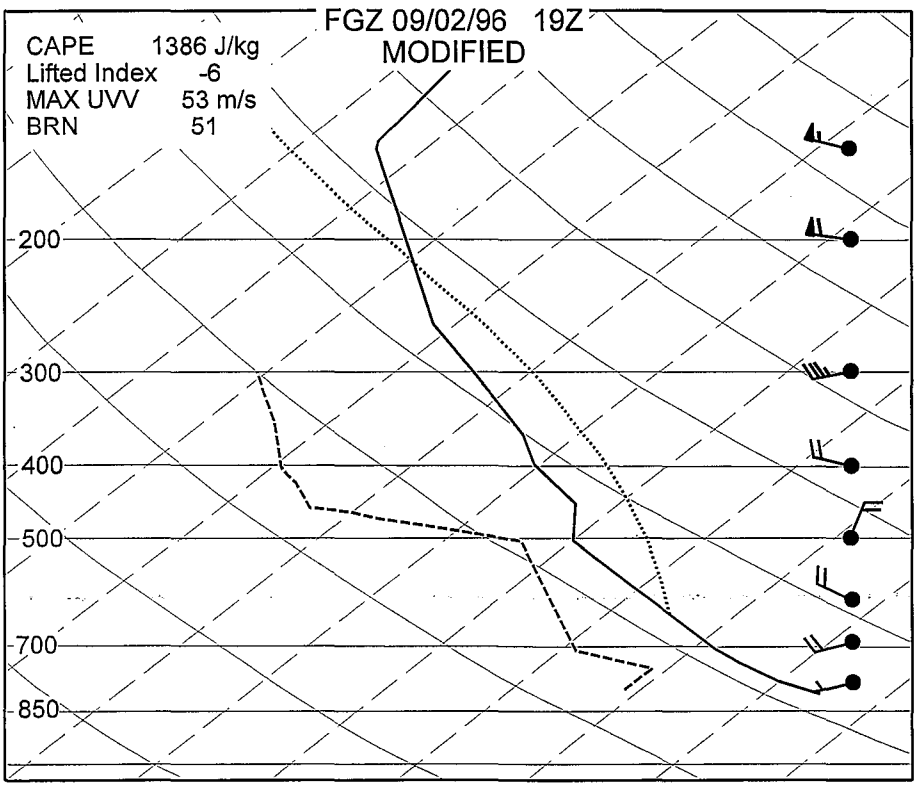

Fig. 4. The observed and modified FGZ soundings valid at 1200 UTC and 1900 UTC, respectively. The dotted line defines the area representing CAPE. The modified sounding was adjusted for surface temperature and dewpoint and boundary layer mixing from the surface to approximately 1 km AGL.

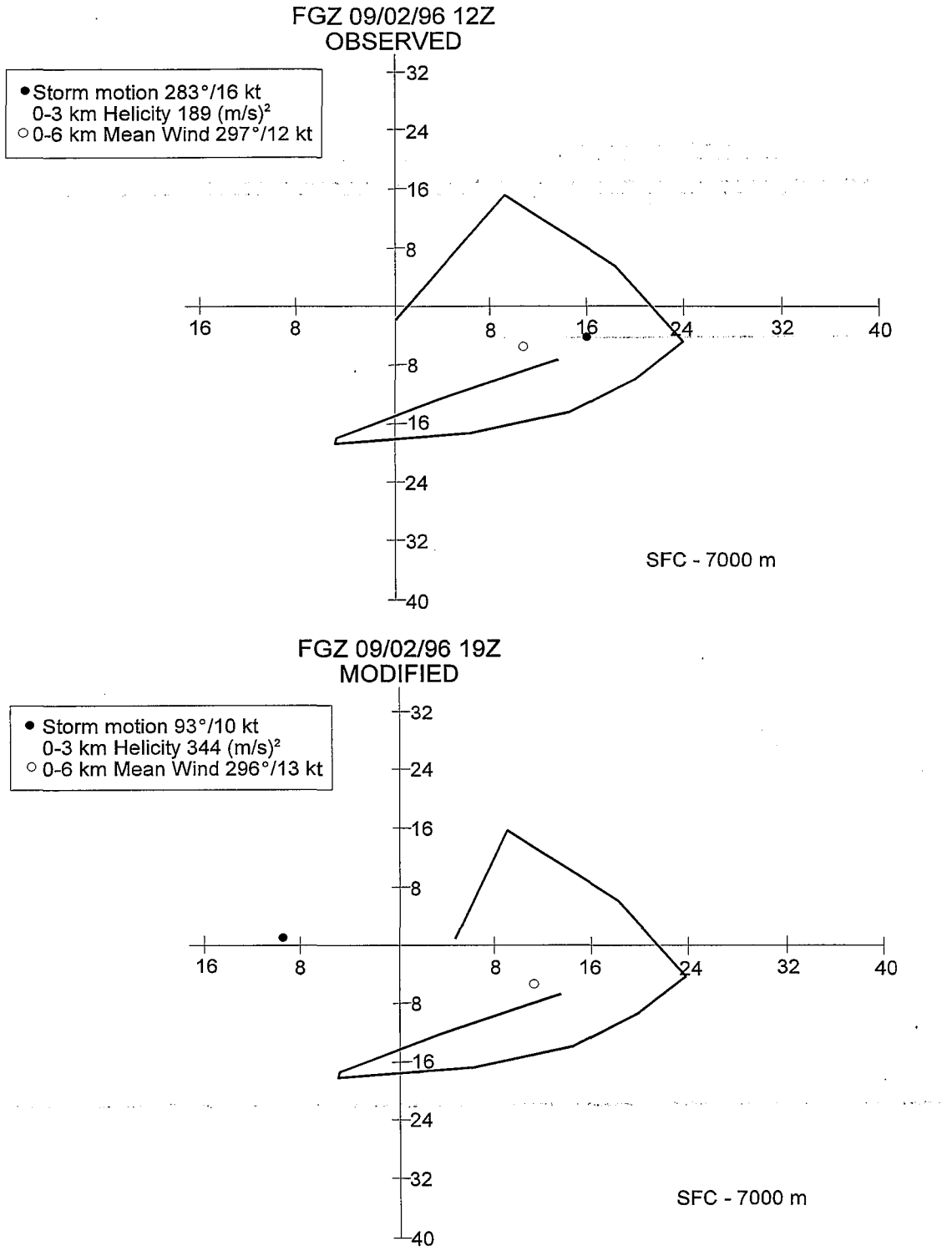

Fig. 5. The observed and modified FGZ hodographs valid at 1200 UTC and 1900 UTC, respectively. The modified hodograph was adjusted for surface wind speed and direction. The open circle (◦) represents the 0-6 km mean wind. The dark circle (•) represents the resulting storm motion.

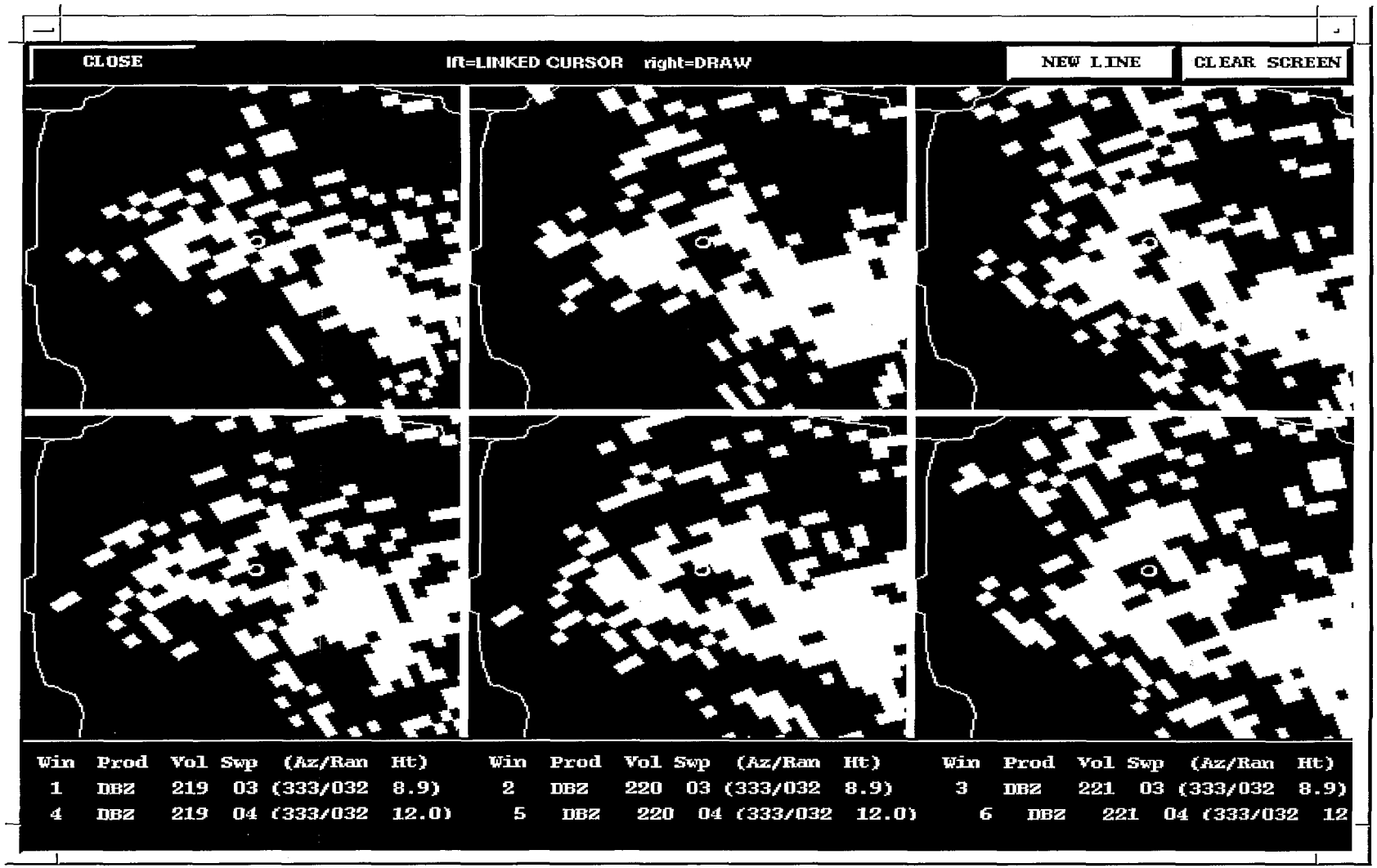

Fig. 6. This figure shows three consecutive volume scans for two different elevation angles sampling the storm at 2970 m and 4000 m AGL. The circle shown in the figures is only a fixed reference point. From volume scans 219 through 221, reflectivities greater than 50 dBZ are shown along an elongated line to the southeast of the reference marker.

Fig. 7. (A) shows evidence of a hook echo (>55 dBZ) to the northwest of the reference marker at an elevation of 970 m AGL. The positions of the main downdraft regions are shown northwest of the white circle and across an area from the north-northeast through southeast. (B) shows greater reflectivity, at an elevation of 6100 m, surrounding the reference marker. A reflectivity v-notch is also shown on the southeast flank of the storm.

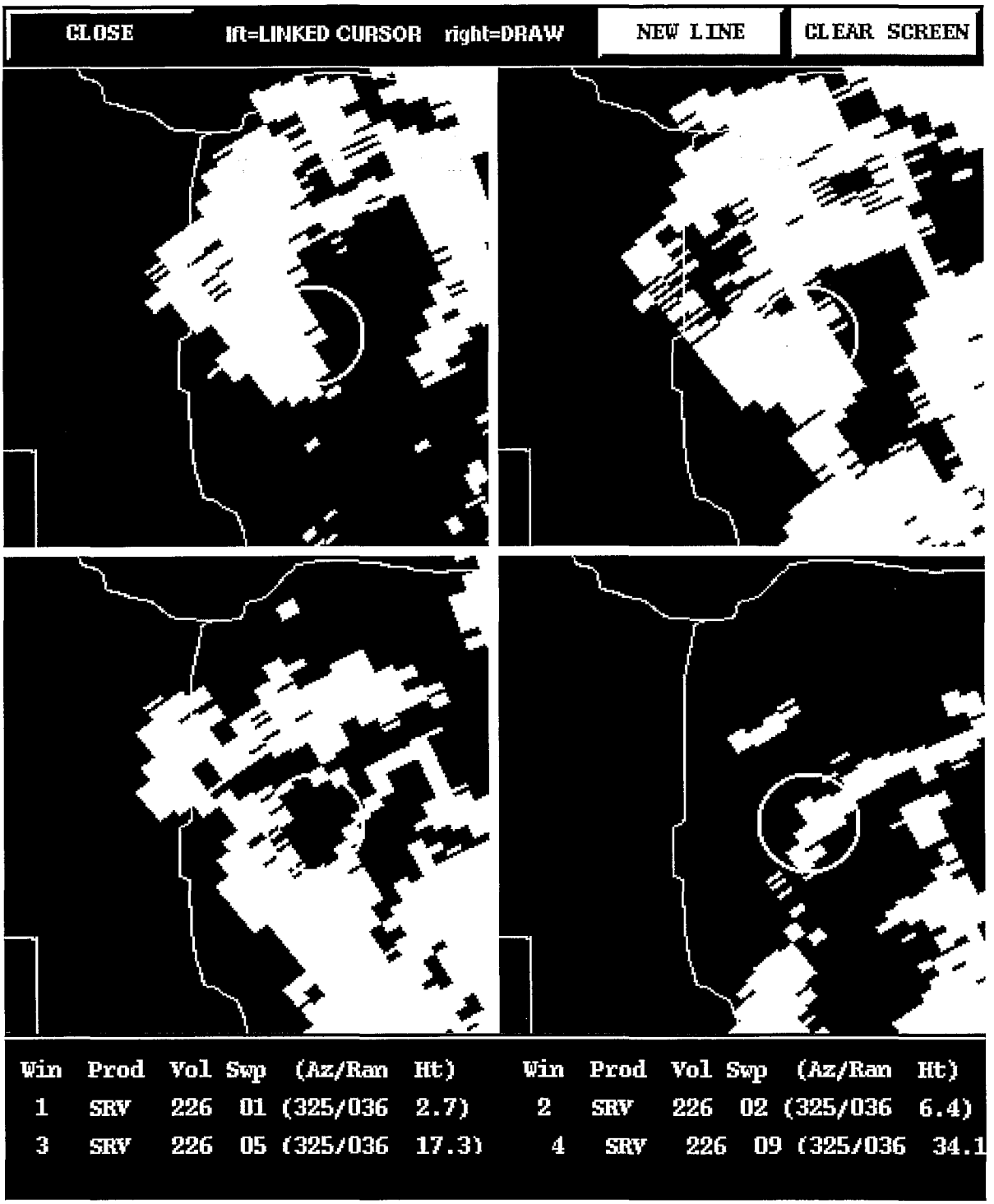

Fig. 8. Storm-relative velocity imagery valid at 2046 UTC shows the earliest stage of the mesocyclone. The top-left panel shows cyclonic curvature at an elevation of 833 m. The top-right and bottom-left panels show cyclonic rotation at elevations of 3166 m and 6533 m, respectively. The bottom-right panel shows divergence near the storm top at 12267 m.

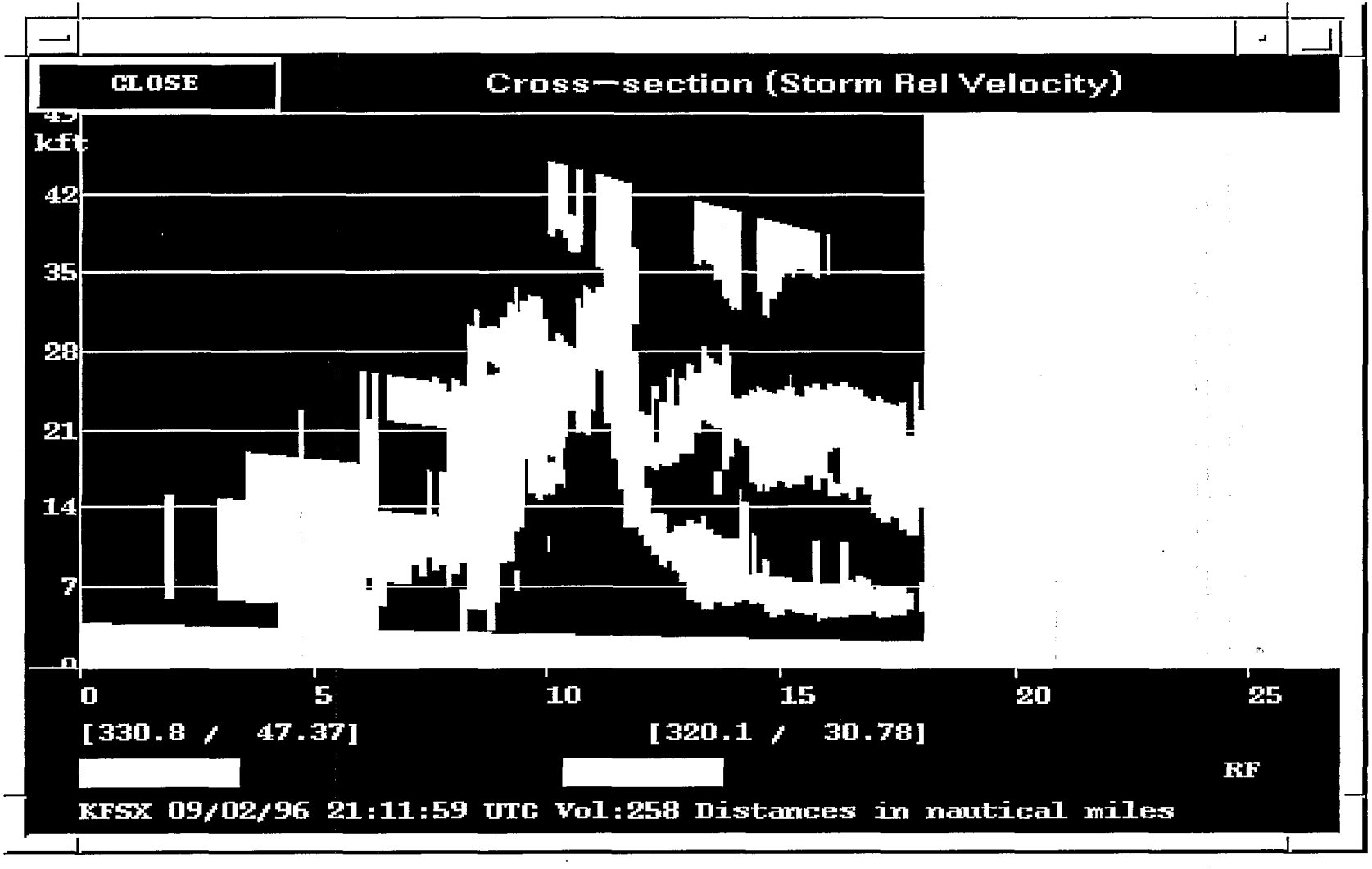

Fig. 9. Storm-relative velocity cross section showing the low-level convergence sustaining the updraft. Near the storm top, strong divergence is shown near 12300 m AGL. This panel is valid at 2112 UTC. The radar is located 90 km to the right of the image.

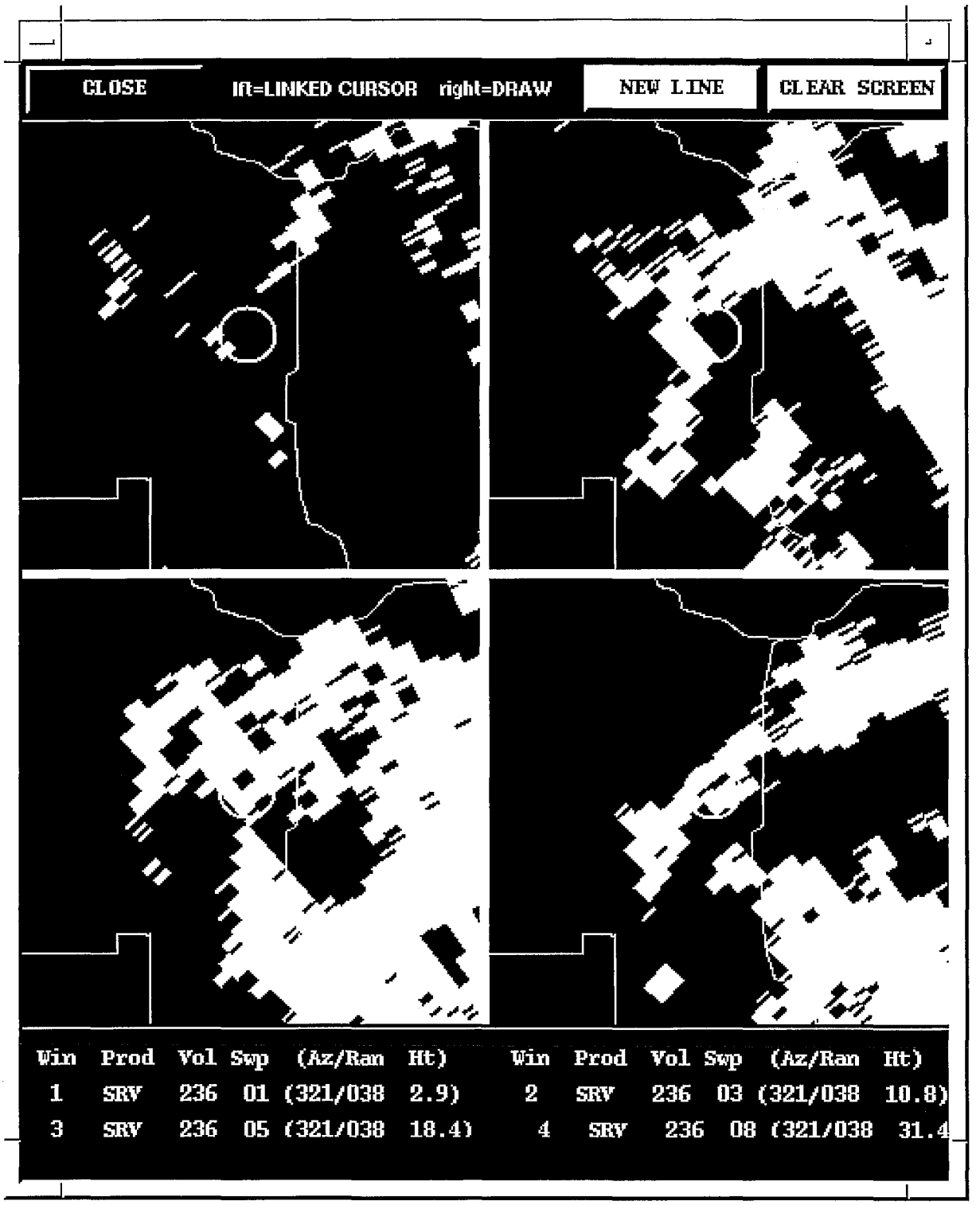

Fig. 10. Four panels depicting storm-relative velocity valid at 2136 UTC. The yellow circle represents the radar identified mesocyclone. The top-left panel shows pure convergence at an elevation of 970 m. The top-right shows cyclonic convergence at 3630 m. At 6200 m, the bottom-left panel shows cyclonic rotation and the last panel, the bottom-right, pure divergence near the storm top of 10570 m was evident.